

# UC Davis

## UC Davis Previously Published Works

### Title

Dispersal, habitat filtering, and eco-evolutionary dynamics as drivers of local and global wetland viral biogeography.

### Permalink

<https://escholarship.org/uc/item/94q856n4>

### Journal

The ISME Journal: Multidisciplinary Journal of Microbial Ecology, 17(11)

### Authors

Ter Horst, Anneliek

Fudyma, Jane

Sones, Jacqueline

et al.

### Publication Date

2023-11-01

### DOI

10.1038/s41396-023-01516-8

Peer reviewed

## ARTICLE



# Dispersal, habitat filtering, and eco-evolutionary dynamics as drivers of local and global wetland viral biogeography

Anneliek M. ter Horst<sup>1</sup>, Jane D. Fudyma<sup>1</sup>, Jacqueline L. Sones<sup>2</sup> and Joanne B. Emerson<sup>1</sup>✉

© The Author(s), under exclusive licence to International Society for Microbial Ecology 2023

Wetlands store 20–30% of the world's soil carbon, and identifying the microbial controls on these carbon reserves is essential to predicting feedbacks to climate change. Although viral infections likely play important roles in wetland ecosystem dynamics, we lack a basic understanding of wetland viral ecology. Here 63 viral size-fraction metagenomes (viromes) and paired total metagenomes were generated from three time points in 2021 at seven fresh- and saltwater wetlands in the California Bodega Marine Reserve. We recovered 12,826 viral population genomic sequences (vOTUs), only 4.4% of which were detected at the same field site two years prior, indicating a small degree of population stability or recurrence. Viral communities differed most significantly among the seven wetland sites and were also structured by habitat (plant community composition and salinity). Read mapping to a new version of our reference database, PIGEONv2.0 (515,763 vOTUs), revealed 196 vOTUs present over large geographic distances, often reflecting shared habitat characteristics. Wetland vOTU microdiversity was significantly lower locally than globally and lower within than between time points, indicating greater divergence with increasing spatiotemporal distance. Viruses tended to have broad predicted host ranges via CRISPR spacer linkages to metagenome-assembled genomes, and increased SNP frequencies in CRISPR-targeted major tail protein genes suggest potential viral eco-evolutionary dynamics in response to both immune targeting and changes in host cell receptors involved in viral attachment. Together, these results highlight the importance of dispersal, environmental selection, and eco-evolutionary dynamics as drivers of local and global wetland viral biogeography.

*The ISME Journal* (2023) 17:2079–2089; <https://doi.org/10.1038/s41396-023-01516-8>

## INTRODUCTION

Wetlands are an important carbon sink, estimated to store between 20 and 30% of the global soil carbon [1]. They also provide ecosystem services, such as flood control, drought prevention, and water quality protection, and they support a rich biodiversity [1–4]. However, these ecosystems are currently being lost at an estimated annual rate of 1.5% globally, releasing stored carbon into the atmosphere [2, 5]. Moreover, due to climate change, soil salinity is increasing in formerly freshwater wetlands, causing changes to microbial and plant communities [6–8] and potentially leading to biodiversity loss [9]. Microorganisms play central roles in carbon turnover and the emission of greenhouse gasses from wetland ecosystems [10], and, by infecting, controlling the metabolism of, and lysing microorganisms, viruses also likely impact these biogeochemical cycles [10, 11]. It is therefore important to characterize fresh- and saltwater wetland microbial and viral communities, in order to understand the ecological and biogeochemical responses of these fragile ecosystems under a changing climate [12–14].

Methodological improvements have only recently made it possible to study soil and wetland viral communities in detail. While some prior efforts focused on bioinformatic mining of viral sequences from total soil metagenomes [15, 16], by purifying the viral size fraction through 0.22 µm filtration prior to metagenomic

sequencing (viromics), a much higher viral diversity can be recovered [11, 17, 18]. Application of these methods to peatlands and a variety of other soils is beginning to reveal ecological factors important to soil viral biogeography, such as soil moisture content, habitat characteristics, and (on local scales) spatial structuring reflecting dispersal limitation and temporal dynamics suggesting responses to fluctuating environments [15–18].

Recent studies have shown substantial differences in soil viral community composition among habitats at both regional and global scales [18, 19]. For example, soil viral 'species' (vOTUs) were rarely shared among four different habitats (grasslands, shrublands, woodlands, and wetlands) in northern California [19], and similarly, few RNA viral sequences were shared between grasslands and peatlands in the United Kingdom [20]. Despite repeated observations of soil viral community heterogeneity at regional or continental scales [21, 22], the same viral species can be found on different continents, usually in the same type of habitat (e.g., peat viruses tend to be restricted to other peatlands) [18]. Although habitat seems to be an important contributor to global soil viral biogeography, the supporting data are sparse; further studies are needed to assess the generalizability of these patterns.

Soil viral community spatial structuring and temporal turnover have also been observed at more local scales, with viral communities showing seasonal dynamics [23] and differing more

<sup>1</sup>Department of Plant Pathology, University of California, Davis, CA, USA. <sup>2</sup>Bodega Marine Reserve, University of California, Davis/Bodega Bay, CA, USA.

✉email: [jbemerson@ucdavis.edu](mailto:jbemerson@ucdavis.edu)

significantly over space and time than bacterial communities [17, 21]. However, those studies were conducted within the same habitat or soil type; differences in viral community composition across habitats have rarely been considered at local scales. In two studies that did compare viral communities by habitat in the same Swedish ecosystem, viral communities were found to be distinct among three habitats along a peatland permafrost thaw gradient [15, 24]. However, those three habitats were also spatially separated, making the relative influences of habitat and spatial location difficult to disentangle. Similarly, viral community compositional differences along a grassland pH gradient also reflected spatial separation, but pH was seemingly the predominant factor driving viral community composition, which was corroborated in a meta-analysis of other soil and peat viral datasets [25]. Disentangling the relative impacts of habitat characteristics, spatial location, and temporal dynamics on soil viral community composition is thus an important near-term goal for advancing the field, but even the appropriate spatiotemporal scales for sampling soil viral communities are unknown.

Building on our prior regional study of 30 viromes from four habitat types with very little overlap in viral species across samples [19], here we hypothesized that reducing complexity from the regional to local scale and restricting the diversity of habitats considered (only wetlands) would yield sufficient vOTU co-occurrence to link viral biogeographical patterns to their potential underlying drivers. We sampled seven different wetland sites across a 0.6 km<sup>2</sup> area at three time points in 2021 at the Bodega Marine Reserve on the California Pacific Coast (USA). We generated 63 viral size-fraction metagenomes (viromes) and 63 total soil metagenomes to profile the dsDNA viral communities and bacterial and archaeal (prokaryotic) communities, respectively, in these wetlands. We also compared results to our viromic dataset from Bodega Bay collected two years prior (in 2019) [19]. Here we explore local and global wetland viral biogeography, investigate which factors among spatial distance, plant and microbial community composition, soil physicochemical properties, and time influence viral community composition, and evaluate the influences of spatial and temporal distance on viral population microheterogeneity and virus-host eco-evolutionary dynamics.

## RESULTS AND DISCUSSION

### Dataset overview

To investigate wetland dsDNA viral biogeography on a local scale, we sampled seven nearby wetland sites within a 0.6 km<sup>2</sup> area in the Bodega Marine Reserve, California, USA (Fig. 1A, map). Sampling sites were initially selected to represent freshwater, brackish, and saltwater wetlands, based on institutional knowledge of plant community composition, and we subsequently measured both plant communities and salinity to empirically define the sampled habitats. Near-surface (top 15 cm) wetland soils were collected at three time points (March, May, and July of 2021), with three samples per time point per wetland site. Samples were collected on average 17 m apart, with the closest samples within a site (regardless of the time point) 1.7 m apart and the farthest 89 m apart (Supplementary Table 1). All 63 samples (7 sites × 3 samples × 3 time points) underwent viral size-fraction metagenomics (viromics) and total metagenomics to measure viral and prokaryotic community composition, respectively. A suite of soil physicochemical properties was also measured for each sample (Supplementary Table 2).

In total, 12,826 viral operational taxonomic units (vOTUs, ≥10 kbp, ≥95% average nucleotide identity, approximately species-level taxonomy [26]) and 219 metagenome-assembled genomes (MAGs, ≥50% complete, ≤10% contaminated [27], Supplementary Table 3) were detected in our samples. From the viromes, we assembled 17,703 viral contigs de novo, which clustered into

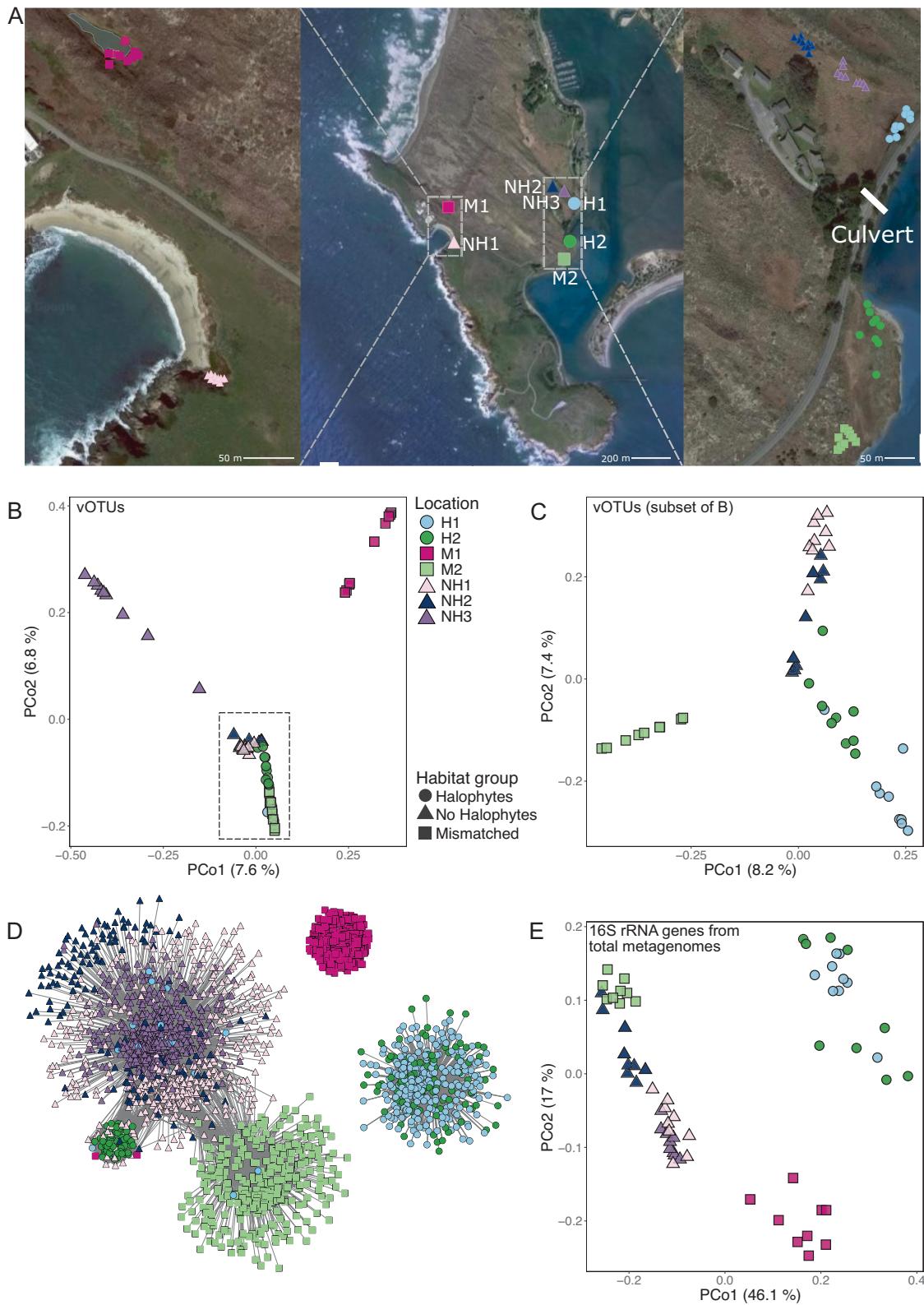
12,261 vOTUs, and we recovered an additional 565 vOTUs by read mapping to our Phages and Integrated Genomes Encapsidated Or Not (PIGEONv2.0) database of 515,763 vOTUs from diverse ecosystems, including 369 vOTUs recovered from Bodega Bay viromes collected in 2019 [19]. Read mapping to these sets of vOTUs and MAGs yielded the estimated relative abundances of each vOTU and MAG in each sample, used for downstream community compositional analyses (Supplementary Tables 4, 5).

### Habitat features (plant community composition and salinity)

We identified 32 plant species across the seven sites (Supplementary Table 6), and plant communities separated the sites into two vegetation groups, based on the presence or absence of halophytes (salt-tolerant plants). There were no overlapping plant species between the two groups, and while most sites in the same vegetation group shared at least one dominant plant species, plant community composition differed at each of the seven sites (Supplementary Table 6). We also used salinity measurements to define habitats, with electrical conductivity measurements ranging from 0 to 82 mmhos/cm in our wetlands, and those between 0 to 2 mmhos/cm considered non-saline, 2 to 4 slightly saline, 4 to 8 moderately saline, 8 to 16 strongly saline, and 16 or greater extremely saline wetlands [28]. Based on these parameters, we separated the seven sites into four habitat groups: “Halophyte (H)” for the two sites with halophyte plants and overall medium to extreme soil salinity (H1 and H2), “No Halophyte (NH)” for the three sites with no halophytes and low to slight soil salinity (NH1, NH2, and NH3), and two “Mismatched (M)” groups (M1 and M2) for two sites for which the vegetation did not correspond with soil salinity. The mismatched (M) sites did not share the same vegetation and salinity mismatch, so they do not represent the same habitat type, leading to four habitat groups (H, NH, M1, M2). Although vegetation tended to be indicative of soil salinity, our salinity measurements varied both within and among sites, and two sites had consistently mismatched salinity and vegetation measurements (site M1 had a ‘no halophyte’ plant community with non-to-strongly saline soils, and site M2 had a “halophyte” plant community with non-saline soils). These seemingly contradictory vegetation and salinity results left us initially concerned that our salinity measurements might have been faulty, but evaporation during dry periods, seasonal waterlogging, precipitation, and leaching of water can all influence soil salinity in short time spans [29]. Halophytic plants outcompete non-halophyte plants in saline environments [30], and coastal salt marshes such as site M2 experience tidal flooding with seawater, leading us to believe that M2 likely sometimes experiences higher soil salinity than we measured, promoting halophyte growth. Halophytes are not competitive in non-saline habitats [31], and since there were no halophytes at site M1 despite the moderate salinity measurements, we speculate that M1 soil is often non-saline.

### Viral and prokaryotic communities were distinct at each of the seven wetland sites but were more similar within than between habitat types

Most (90%) of the vOTUs were uniquely identified in only one of the seven wetland sites. While 38% of the vOTUs were detected in only one of the 63 viromes (Supplementary Fig. 1), the proportion of these single instance vOTUs was substantially reduced, compared to our prior regional-scale comparison of 30 viromes across grassland, shrubland, woodland, and wetland habitats, in which 81% of the vOTUs were detected in only one virome [19]. Thus, the localized focus in one area and restriction to wetland habitats here, as well as increased spatiotemporal resolution, improved our ability to identify vOTUs shared across samples, as is necessary for recognizing biogeographical patterns. Of the 62% of vOTUs detected in more than one virome, 6680 (52%) were recovered only within one wetland site, and viral community composition was significantly different at each site (PERMANOVA



$p < 0.001$ , Fig. 1B, C). The average pairwise Bray-Curtis dissimilarity between viromes from the same site at the same time point versus at different time points was not significantly different ( $T$  test,  $p = 0.26$ ), indicating that viral community compositional differences over space were just as substantial as differences over time, so samples from the same time point at the same site were

statistically treated as individual samples, rather than biological replicates. The PCoA plots (Fig. 1B, C) explained a relatively small percentage of the variance in viral community composition, which we think is attributable to very high viral community beta-diversity in the dataset, including within each site, as shown in Supplementary Fig. 1. Viral community beta-diversity was

**Fig. 1 Sampling design and overarching compositional patterns for Bodega Bay viral and prokaryotic communities.** **A** Sampling locations for all Bodega Bay samples. Center: locations of the seven wetland sites within the Bodega Marine Reserve, Left and Right: locations of each of the nine samples per site (a zoomed in view of each site with individual sample labels is in Supplementary Fig. 1). Per the legend below the images, circles correspond to locations with halophyte vegetation and saline soils, triangles correspond to locations without halophytes and non-saline soil, and squares correspond to mismatched locations. The 'culvert' label indicates the location of a human-made pipe below the road that allows for water movement. **B, C** Principal coordinates analysis (PCoA), based on Bray-Curtis dissimilarities derived from the table of vOTU abundances (read mapping to vOTUs). Each point is one sample (one virome), with viral communities from **(B)** all 63 viromes, and **(C)** the 45 viromes indicated by the dashed rectangle in **(B)**. Panel **(C)** is a new PCoA to better show separation among overlapping samples in **(B)**. **D** Co-occurrence network of vOTUs detected in more than one Bodega Bay virome, colored by the site in which they were most abundant (had the highest average per-bp coverage depth). Nodes represent vOTUs, and edges represent a significant co-occurrence between the vOTUs, calculated using a probabilistic co-occurrence model with the R package *cooccur*. **E** PCoA based on Bray-Curtis dissimilarities of 16S rRNA gene OTU community composition, where 16S rRNA gene reads were bioinformatically mined from 63 total metagenomes. For all PCoA plots **(B, C, E)**, the percent variance explained by each axis is indicated in parenthesis.

significantly negatively correlated with the pairwise spatial distance between samples (Supplementary Fig. 2A), implicating dispersal limitation as one potential driver of these patterns (as also suggested in previous work [17, 19, 21]). Specifically, viral community Bray-Curtis dissimilarity scores increased on average by 0.13 (out of a maximum dissimilarity score of 1) per 10 meters between samples (Supplementary Fig. 2A).

Despite overarching differences among wetland sites, viral communities grouped secondarily according to habitat type (Fig. 1B, C), with significant differences among the four habitat groups (H, NH, M1, and M2, PERMANOVA,  $p < 0.001$ ). Consistent with edaphic factors as potential drivers of these differences, viral community composition correlated significantly with plant community composition, microbial community composition, and soil chemical measurements (Supplementary Fig. 2B, Supplementary Table 2), such as pH, moisture content, and sulfate concentrations (Supplementary Fig. 2C). Microbial community composition also correlated significantly with plant community composition and various soil chemical measurements. A BIO-ENV analysis indicated that soil potassium and calcium correlated best with viral community composition ( $R^2 = 0.53$ ,  $p = 0.001$ ). These results are similar to those from a California grassland, in which calcium, zinc, and potassium concentrations were significantly correlated with viral community composition [21]. Considering only between-habitat beta-diversity, the viral communities from sites NH1 and NH2 were the most similar (Fig. 1C), despite being physically far apart (Fig. 1A), perhaps related to their similar salinity and plant communities (Supplementary Table 6). This is consistent with prior work that has suggested that plant cover type could play an important role in shaping soil viral communities [32]. Similar salinity and plant communities were likely also drivers of viral community compositional similarity at sites H1 and H2. Those sites are also connected by a culvert (a human-made water tunnel beneath a road) (Fig. 1A), presumably facilitating dispersal between the sites. Finally, the two mismatched sites each had distinct viral communities, potentially due to their unique combinations of plant composition and salinity.

A co-occurrence analysis revealed that vOTUs were most often shared across samples from the same habitat type. Specifically, vOTUs from all three non-halophyte soils (NH1, NH2, and NH3) tended to co-occur, as did vOTUs from wetlands with halophyte plants (H1 and H2). Perhaps reflecting the lack of other samples from the same habitat types in this dataset, vOTUs from each of the mismatched sites tended to co-occur only with other samples from the same site, but a small subnetwork of vOTUs from the halophyte site H2 co-occurred with vOTUs from the non-halophyte wetlands. All of those co-occurring vOTUs were either the most abundant in or only detected in one particular H2 sample, H2-1-T2, which had low salinity (1.69 mmho/cm) (Supplementary Table 2). This suggests that environmental selection (presumably by way of microbial hosts) can act on wetland viral communities on very short time scales, and/or that an influx of new vOTUs was brought to site H2, being already

adapted to conditions in the less saline water that brought them there.

The two sites with the most within-site vOTU co-occurrences (NH3 and M1) also had the highest moisture content, consistent with hydrological mixing facilitating greater viral community homogeneity. Specifically, site NH3 harbored viral communities distinct from all other sites (Fig. 1B), despite its similar salinity and plant community composition to the other two non-halophyte sites and its close proximity to NH2 (Fig. 1A, Supplementary Table 2). A comparatively large percentage of vOTUs was shared across samples within the NH3 site (35% of vOTUs were shared among five or more NH3 samples, relative to only 8% on average for the other two non-halophyte sites, Supplementary Fig. 1). Similarly, communities from site M1 were also distinct, with 30% of their vOTUs detected in five or more samples from the same site, whereas the five other sites (not NH3 or M1) shared only 9% of their vOTUs across five or more samples from the same site. Soil moisture content was highest at sites NH3 (83% on average) and M1 (52% on average), compared to 34% on average at the other five sites, likely facilitating more mixing and greater viral community homogeneity due to greater hydrologic connectivity. Overall, the viral community compositional and vOTU co-occurrence patterns revealed both dispersal (and dispersal limitation) and environmental selection (biotic and abiotic habitat characteristics) as likely drivers of local wetland viral biogeographic patterns.

To determine whether prokaryotic communities exhibited similar patterns to the viral communities, prokaryotic community composition and co-occurrence were also investigated. Briefly, the relative abundances and co-occurrences of MAGs and, separately, of 16S rRNA gene reads recovered from total metagenomes were used for these analyses. While most of the prokaryotic communities were significantly different at each of the wetland sites (Fig. 1E, Supplementary Fig. 3A), the communities from the Halophyte sites (H1 and H2) were not significantly different from each other (PERMANOVA,  $p = 0.055$ ), grouping more by habitat type than did the viral communities. Co-occurrence networks for MAGs showed similar patterns to those of the viral communities, largely reflecting shared MAGs within the same habitat type, though relatively few MAGs were recovered from the non-halophyte wetlands (Supplementary Fig. 3B, C). Although read-based 16S rRNA gene OTUs also showed the most co-occurrence within habitat types, OTUs were detected in multiple habitats far more often than were MAGs, suggesting that increased resolution (i.e., not requiring assembly into MAGs) revealed more co-occurrence, presumably due to increased access to both rare community members and taxa with genomes that did not assemble well [33]. Overall, patterns for prokaryotic communities were similar to those of their viruses, and viral community composition was significantly correlated with prokaryotic community composition (Mantel test,  $p < 0.001$ ), suggesting that at least some of the observed viral biogeographical patterns were due to habitat filtering (environmental selection) by way of their hosts.

**Global distribution patterns for Bodega Bay vOTUs suggest that wetland viral biogeography reflects habitat and salinity** To compare vOTUs recovered at Bodega Bay to the global viral metacommunity, we leveraged a new version of our Phages and Integrated Genomes Encapsidated Or Not (PIGEONv2.0) database, which we introduce here. Since the first iteration of PIGEON (PIGEONv1.0), which contained 266,125 vOTUs [18], PIGEONv2.0 has almost doubled in size, now including 515,763 vOTU sequences. The number of soil vOTUs increased from 15,892 to 61,757, predominantly from our in-house soil viromics data, including previously unpublished datasets that we are now making publicly available in PIGEONv2.0. The number of freshwater vOTUs also substantially increased, largely due to the addition of viruses from aquatic viromes from Lake Baikal in Russia [34]. Here, these PIGEON improvements have facilitated global comparisons of Bodega Bay vOTU occurrence patterns.

Of the 12,826 vOTUs recovered at Bodega Bay, 196 (1.5%) were previously detected at other sites throughout the world (Fig. 2A), recovered here through read mapping to PIGEONv2.0 (Fig. 2B, Supplementary Table 7). Bodega Bay vOTUs were previously recovered from non-wetland soils (83), freshwater lakes (57), marine ecosystems (33), non-peat freshwater wetlands (14), and peat wetlands (8), indicating globally present viruses in relatively similar ecosystems throughout the world (Fig. 2A, Supplementary Fig. 4A). Notably, zero vOTUs from human-associated habitats were detected in these wetlands, perhaps indicating species boundaries between these very different habitat types, though we

also note that our focus in developing PIGEON has been on environmental viruses, with only 15,235 human-associated vOTUs in the database. Most vOTUs that were detected in non-saline or slightly saline wetlands at Bodega Bay were originally recovered from non-wetland soils (62) or freshwater ecosystems (46), whereas most vOTUs from saline wetlands were previously recovered from marine (34) or non-wetland soil (28) ecosystems (Supplementary Fig. 4B), again suggesting that habitat characteristics underlie global viral biogeographic patterns. Similarly, we also considered the relationship between vegetation group at Bodega Bay and the habitat in which a given vOTU was originally recovered (Fig. 2D) and found that vOTUs from the non-halophyte sites were most often previously detected in non-wetland soils (79) or freshwater ecosystems (57), while vOTUs from the halophyte sites were most often previously detected in marine ecosystems (24) (Fig. 2C). Together, these results indicate that habitat characteristics—in this case, salinity and salinity indicators (halophyte or non-halophyte plant community composition)—can drive wetland viral community biogeography on a global scale.

### Wetland viral microdiversity was lower locally than globally and lower within than between time points

To investigate the contributions of viral genotypic heterogeneity to local and global viral ecology, we used inStrain [35] to calculate vOTU microdiversity profiles and compared dominant allelic variants over time and space. Specifically, we compared vOTU reference sequences initially recovered from PIGEONv2.0 (not

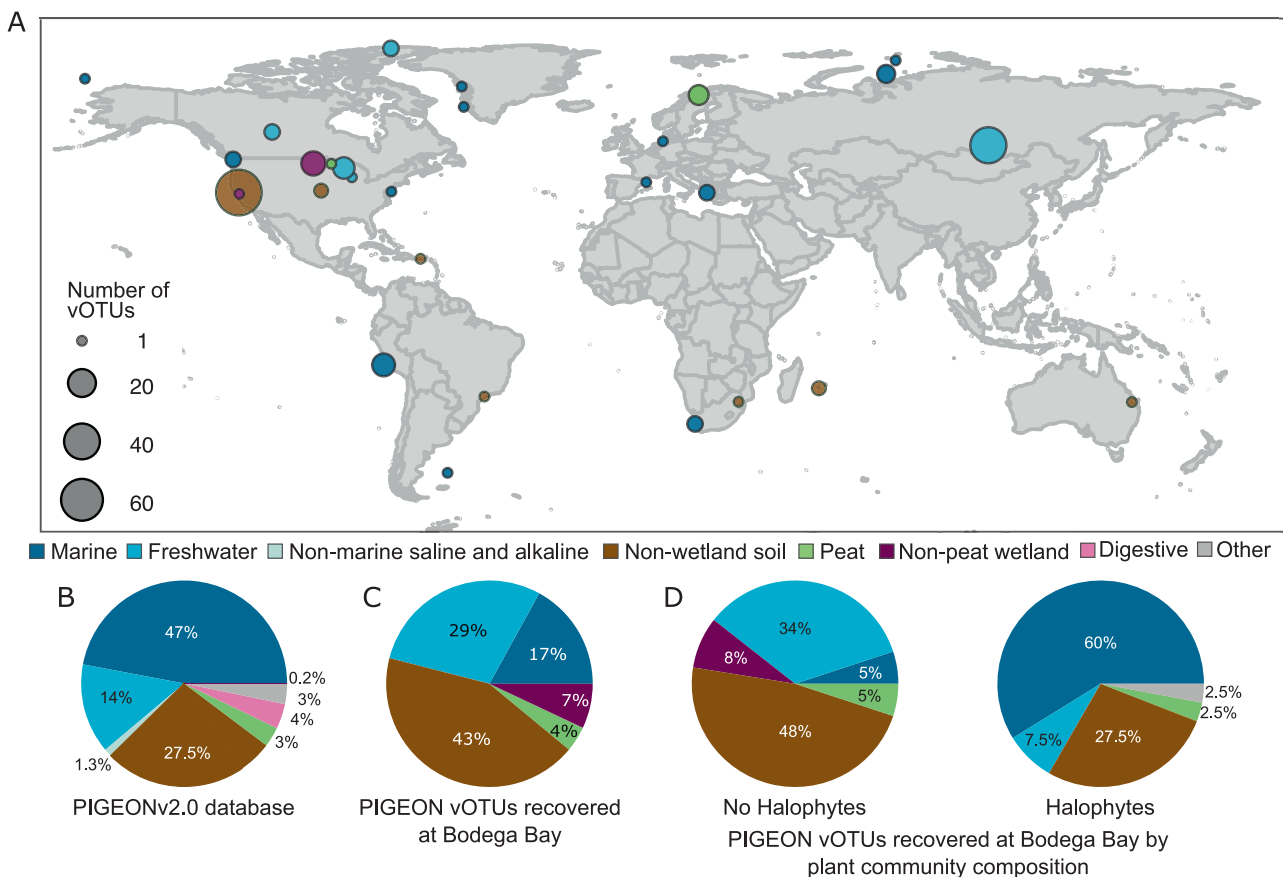


**Fig. 2** Global distribution and habitat context of Bodega Bay vOTUs, leveraging the PIGEONv2.0 database. **A** vOTUs ( $n = 196$ ) from PIGEONv2.0 recovered at Bodega Bay by read mapping, according to the location where they were first recovered, colored by the environment in which they were originally recovered. Circle size indicates the number of vOTUs. **B** Composition of the PIGEONv2.0 database of 515,763 vOTU sequences, colored by environment. **C** Relative proportions of all vOTUs recovered from PIGEONv2.0 at Bodega Bay, colored by the original environment from which they were recovered. **D** Relative proportions of vOTUs recovered from PIGEONv2.0 at Bodega Bay, as in panel (C), but separated by the Bodega vegetation group in which they were recovered, colored by original source environment. If a vOTU was recovered in both vegetation groups, it appears twice in the chart.

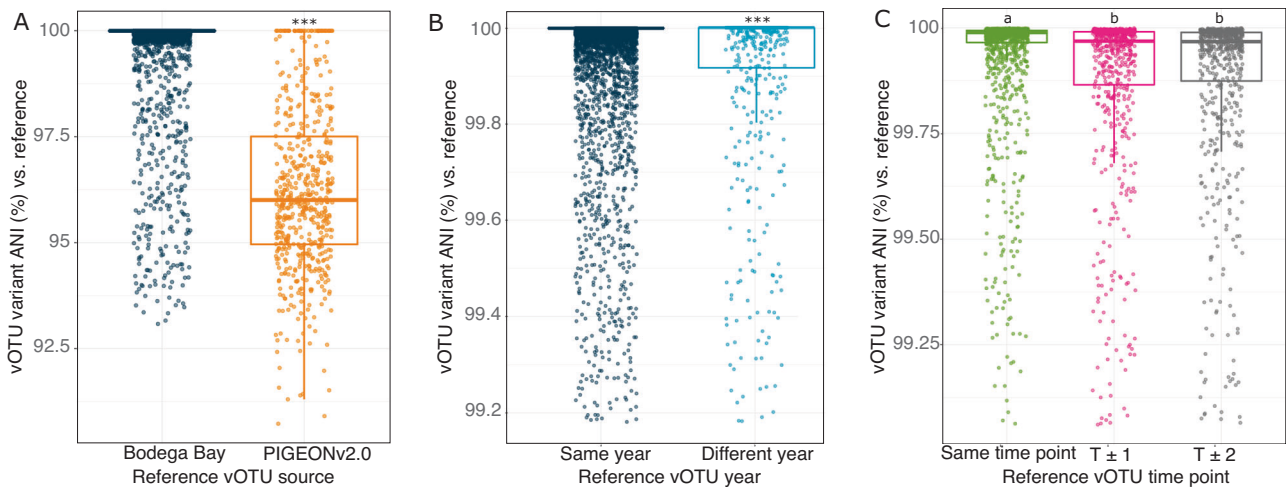


**Fig. 3 Comparisons of viral variant (sub-population) diversity in local and global contexts.** Pairwise average nucleotide identities (ANIs) between vOTU variants, calculated between each sample-specific vOTU consensus sequence and the originally assembled (reference) vOTU sequence, using inStrain. Each point is the ANI for one vOTU variant in one Bodega Bay virome compared to the reference sequence for that vOTU. **A** Variant ANIs for: (left) vOTUs both assembled and recovered through read mapping from the Bodega Bay dataset (Bodega Bay reference sequences), and (right) vOTUs recovered at Bodega Bay via read mapping but originally derived from PIGEONv2.0 (PIGEONv2.0 reference sequences). Stars above boxes correspond to significant differences between groups (Student's *T* test, significant when  $p < 0.001$ ). **B** Variant ANIs for vOTUs both assembled and recovered via read mapping from Bodega Bay, either: (left) assembled and recovered in the same year (2019-2019 or 2021-2021), or (right) in different years (2019-2021 or 2021-2019). **C** Variant ANIs for vOTUs assembled from Bodega Bay in 2021, either assembled and recovered through read mapping at the same sampling time point, or at different time points, where  $T \pm 1$  equals 2 months between samplings, and  $T \pm 2$  equals 4 months. Only pairs of samples from the same wetland site were considered in this analysis. Letters above boxes correspond to significant differences between groups (Student's *T* test, significant when  $p < 0.001$ ). In all three panels, boxes show the median and interquartile range (IQR), and whiskers extend to  $Q1 - 1.5 \cdot IQR$  and  $Q3 + 1.5 \cdot IQR$ .

assembled from Bodega Bay, 196), assembled from Bodega Bay in 2019 (2377) [19], and assembled from Bodega Bay in 2021 (this study, 12,261) to their variants recovered in different samples at Bodega Bay. As these vOTUs were derived from consensus assembly sequences, representing composite genomes, highly variable regions of the genome are less likely to be included in the consensus sequence, so these microdiversity results are likely skewed towards measurements within the more conserved regions of the viral genomes. For each vOTU, we calculated pairwise average nucleotide identities (ANIs) between each sample-specific consensus variant sequence from Bodega Bay and the reference vOTU sequence. Genomic similarity between Bodega Bay variants and PIGEON references was significantly lower on average (average ANI 97.48%) than that for variants that were both assembled and recovered from Bodega Bay (average ANI 99.55%, Fig. 3A,  $p < 0.001$ , Student's *T* test). Given the global scale of PIGEON and local scale of Bodega Bay, this indicates greater viral population allelic variance (genomic heterogeneity) with increasing distance and/or time between samplings, a pattern known as 'isolation by distance' that has been studied for geographic distance, whereby populations in closer proximity are more genetically similar than populations that are farther away [36].

A relatively small number of the Bodega Bay vOTUs detected in 2021 were also recovered from Bodega Bay in 2019 (568 vOTUs, 4.4% of the 2021 dataset). This suggests that a small part of the wetland soil virosphere was stable or consistently recurrent over time. However, for vOTUs that were assembled and recovered through read mapping in the same year, the genomic similarity of dominant allelic variants was higher (99.86%) than for vOTUs that were assembled and recovered in different years (99.25%, Student's *T* test,  $p < 0.001$ , Fig. 3B). Thus, although these viral species persisted over time, their strain-level heterogeneity increased over the two years, consistent with temporal "isolation by distance" [36], with populations farther apart in time exhibiting more genomic divergence.

Sub-population dynamics for vOTUs that were recovered multiple times within the same Bodega Bay wetland site in 2021

were also compared to assess short-term eco-evolutionary dynamics. Genomic similarity of dominant allelic variants was highest for vOTUs recovered through read mapping at the time point from which they were assembled (Fig. 3C) and was significantly lower at both of the other time points. This indicates that, even over short time scales of two to four months, variants significantly fluctuated in abundance and/or diverged. Given that there was no linear trajectory in variant ANI divergence with time (variants were just as different between adjacent time points as between the first and third time points), it is possible that abundance fluctuations could explain these patterns better than iterative divergence, but greater temporal resolution would be needed to bolster that interpretation.

We also used inStrain to compare MAG allelic variants in the 2021 Bodega Bay dataset. MAG variants recovered and assembled at the same time point were most genomically similar (had the highest ANI), whereas MAGs from different time points had significantly lower ANI (Supplementary Fig. 3D). Interestingly, in contrast to the vOTU variants, MAG sub-population dynamics exhibited temporal progression, with sub-population pairs from the same time point most similar, those from the first and last time points most distinct, and those from adjacent time points (i.e., from time points 1 and 2 or 2 and 3) exhibiting intermediate similarity in their ANIs. Additional time points would be required to determine whether this is likely due to divergence over time, but results show sub-population dynamics for both viral and prokaryotic populations over months.

### vOTUs tended to have broad predicted host ranges, and on average, MAGs had evidence for past interactions with more than 10 vOTUs

To investigate putative host ranges, we bioinformatically linked vOTUs to MAGs, using CRISPR arrays [37]. All 12,826 vOTUs and 219 MAGs (210 Bacteria and 9 Archaea) were used for this analysis. A total of 29,709 CRISPR arrays was recovered from the metagenomes, and 683 virus-host linkages were predicted between 378 vOTUs and 53 MAGs. All identified host MAGs were

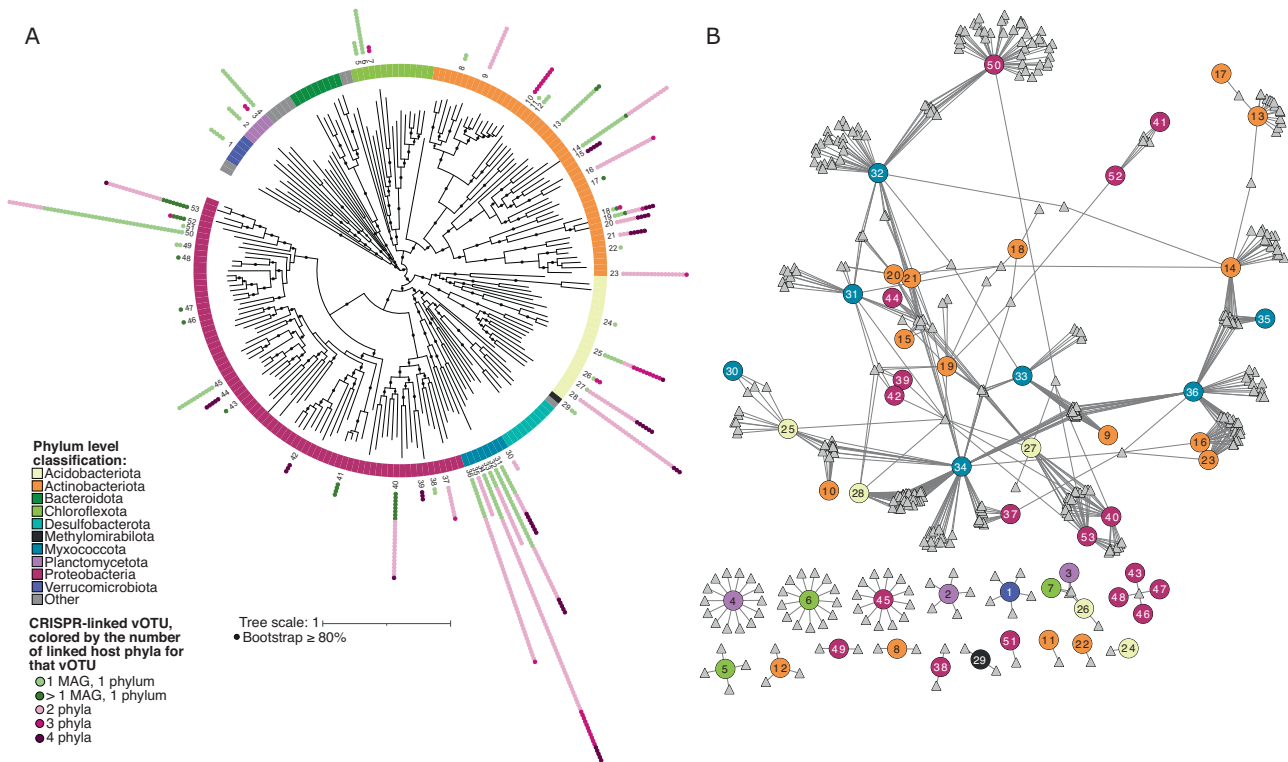


**Fig. 4 Bodega Bay virus-host linkages and putative interactions derived from CRISPR spacer-protospacer matches.** **A** Unrooted phylogenetic tree (concatenated predicted protein alignment of 43 marker genes defined by CheckM) of prokaryotic metagenome-assembled genomes (MAGs) with at least one vOTU linked by CRISPR sequence homology. The numbers for MAGs correspond to numbers in panel (B). Tree was constructed using GTDB-Tk under the WAG model. **B** Virus-host linkage network for MAGs with at least one vOTU linked through CRISPR homology. Circle nodes represent MAGs and are colored by phylum, while triangles represent vOTUs.

bacteria and could be classified to at least the phylum level, with *Proteobacteria* and *Actinobacteriota* among the most commonly reconstructed MAGs (Fig. 4A). Since the number of linkages was low, we also attempted to run iPHoP [38] for additional virus-host linkages, and hosts were predicted for an additional 247 vOTUs. Of these linkages, 204 (82.6%) were to bacteria from the *Actinobacteriota* ( $n = 132$ ) and *Proteobacteria* ( $n = 72$ ). Samples from medium to extremely saline wetlands had significantly more CRISPR arrays and spacers than others, perhaps suggesting increased viral predation, but there was no significant relationship between the number of CRISPR arrays or spacers and the number of vOTUs in a given sample (Supplementary Fig. 5). Previous research has shown that there is a relationship between environment and CRISPR-Cas prevalence, where environment type (e.g., saline versus non-saline environments) accounted for approximately 22% of the variation in prevalence [39]. A positive correlation between viral abundance and CRISPR-spacer abundance was also found in that study, with CRISPR spacers more abundant when viral diversity was lower, but we were not able to detect these trends in our data, perhaps due to differences in dataset sizes and/or ecosystems studied. The average MAG was linked to 13 vOTUs in our dataset, indicating that wetland prokaryotic populations can be infected by (or otherwise interact with [40]) multiple, diverse viral species. On average, each vOTU was linked to four MAGs, and 164 vOTUs (45% of those with predicted hosts) had putative linkages to MAGs in different phyla (Fig. 4A, B). The average vOTU was linked to MAGs in two phyla, and, when only considering vOTUs linked to more than one MAG, vOTUs were linked to MAGs across three or more phyla on average.

These results suggest either that CRISPR spacer matches to viral proto-spacers are imperfect for predicting virus-host linkages associated with infections in these systems, or that wetland

viruses have much broader host ranges than previously appreciated. Recent studies have suggested that viral interactions with hosts may be far less specific than previously understood, with viruses infecting (or otherwise interacting with) prokaryotes across different phyla [17, 40, 41]. The mechanisms that could routinely enable viruses to infect different phyla are unknown, but recent evidence for diverse plasmid-dependent phages [42] (which target conjugation proteins encoded by horizontally transferrable plasmids) offers one interesting possibility for cross-infection that bears further exploration. Cross-phylum CRISPR linkages could also reflect non-specific interactions (e.g., uptake of viral particles or DNA by non-primary hosts, or horizontal transfer of CRISPR regions), as opposed to infections, and these interactions have been suggested to be more common than previously appreciated [40].

To investigate viral evolution in response to host immunity, we calculated the allelic variance within and outside of the viral genomic regions linked to CRISPR spacers, using the originally assembled vOTU sequence as the reference for SNP identification for each vOTU. Viral genomic regions with a CRISPR-spacer match had on average 5.6 SNPs/Kbp, whereas the genome outside of the match had on average 3.3 SNPs/Kbp, indicating more allelic variance in CRISPR-targeted regions, compared to the rest of the viral genome. This has been seen previously, for example in *Streptococcus thermophilus* phage-host coevolution experiments and in an acid mine drainage system [43, 44], and it suggests increased phage genome diversification in CRISPR targeted regions to promote immune evasion. Of the predicted proteins in the CRISPR-targeted viral genomic regions with SNPs, 87% were annotated as hypothetical proteins, and 9% were putative major tail proteins. A significantly larger proportion of putative tail proteins was found in these regions than was annotated as putative major tail proteins in the whole dataset



(0.93%,  $p < 0.00001$ , Z-test). This suggests that there is selection for accelerated evolution in viral genomic regions targeted by CRISPRs, particularly in tail proteins likely involved in attachment to host cell receptors [45]. Evidence for higher mutation rates in phage tail protein genes is presumably due to viral adaptation to changes in host cell receptors to facilitate attachment, as previously suggested [46, 47].

## CONCLUSIONS

We analyzed dsDNA viral communities from the Bodega Bay, California wetland ecosystem and showed significant differences in viral community composition across seven wetland sites, with evidence for dispersal, dispersal limitation, and habitat filtering as underlying drivers of the observed patterns. Although wetland viral communities differed predominantly by location within Bodega Bay, perhaps reflecting local dispersal limitation, the two wetland sites with the most homogeneous communities had the highest soil moisture content, suggesting hydrologic mixing and more opportunities for within-site dispersal with increasing moisture content. Local wetland viral communities were secondarily structured by habitat characteristics, such as plant community composition and soil salinity, indicating environmental filtering, perhaps by way of host adaptation. A small fraction (1.5%) of the vOTUs were previously recovered elsewhere, with global biogeographical patterns largely linked to habitat characteristics; marine vOTUs tended to be recovered in saline wetlands, freshwater vOTUs in non-saline wetlands, and soil vOTUs across wetland habitats.

In addition to dispersal and environmental filtering, eco-evolutionary dynamics (e.g., diversification and/or compositional shifts among dominant allelic variants) contributed to local and global viral biogeographical patterns. Pairwise ANI % between dominant allelic variants (sub-populations) differed significantly between years and over the four-month timescale of this study. In addition, Bodega Bay vOTU variants tended to be more divergent from reference vOTUs recovered elsewhere globally than from reference sequences assembled from Bodega Bay. The observed greater divergence over larger spatiotemporal scales is consistent with patterns of 'isolation by distance', whereby variants closer together in time and/or space likely had greater opportunities for gene flow. On a global scale, this may reflect local diversification and global dispersal limitation of most variants. Our limited ability to link viruses to their hosts (a limitation of the current state of the field) makes the contributions of virus-host co-evolutionary dynamics to biogeographic patterns difficult to evaluate, but we did see evidence for virus-host interactions spanning multiple phyla. Taken together, these results highlight dispersal, environmental filtering, and eco-evolutionary dynamics as likely drivers of both local and global wetland viral biogeographical patterns, expanding our understanding of the highly diverse and dynamic global soil virosphere.

## METHODS

### Field site and sample collection

Samples were collected three times over four months at the University of California, Davis Bodega Marine Reserve, in seven wetland soil ecosystems within the reserve (Supplementary Table 2). Sample collections were performed on March 17th, May 13th, and July 15th, 2021 (T1, T2 and T3, respectively) from each of seven distinct wetland sites. The plant community at each site was used as an indicator for soil salinity (Supplementary Table 6), such that the seven wetland sites were initially selected to represent three low-salinity and four high-salinity habitats, but subsequent analyses revealed more nuance in these habitat types (see main text). At each time point, three surface soil samples (0–15 cm deep, 2.5 × 2.5 cm square area) were collected per wetland site, using a soil knife. The soil within each sample was homogenized and stored at –80 °C until further processing.

### Virome DNA extraction, library construction, and sequencing

Soil virions were enriched using a modified version of a previously published protocol [48]. For each sample, 10 g of soil were suspended in 30 mL of protein-supplemented phosphate-buffered saline solution (PPBS: 2% bovine serum albumin, 10% phosphate-buffered saline, 1% potassium citrate, and 150 mM MgSO<sub>4</sub> in ultrapure water), briefly vortexed, placed on an orbital shaker (30 min, 400 rpm, 4 °C), and then centrifuged (10 min, 3095 × g, 4 °C). Supernatant was then centrifuged twice (8 min, 10,000 × g, 4 °C) to remove residual soil particles. The purified supernatants were then filtered through a 0.22 μm polyethersulfone membrane to remove most cells. The resulting filtrate was ultracentrifuged (2 h 25 min, 32,000 rpm, 4 °C) to pellet the virions, using an Optima LE-80K ultracentrifuge with a 50.2 Ti rotor (Beckman-Coulter Life Sciences). Supernatants were decanted, and pellets were resuspended in 100 μl of ultrapure water. DNase treatment was not performed, as soil samples were stored frozen prior to processing, due to COVID-19 lockdown restrictions, and avoiding DNase treatment on such samples has been shown to improve viromic DNA yields without substantially compromising the viral 'signal' in the data [49]. DNA was extracted from the virus-enriched fraction, using the DNeasy PowerSoil Pro kit (Qiagen, Hilden, Germany), following the manufacturer's instructions, with an added step of a 10-min incubation at 65 °C before the bead-beating step. Libraries were constructed by the UC Davis DNA Technologies Core, using the DNA Hyper Prep library kit (Kapa Biosystems-Roche, Basel, Switzerland), and paired-end 150 bp sequencing was done using the NovaSeq S4 platform (Illumina) to an approximate depth of 10 Gbp per virome.

### Total DNA extraction, library construction, and sequencing

Total DNA was extracted from 0.25 g of soil per sample with the DNeasy PowerSoil Pro kit (Qiagen, Hilden, Germany), following the manufacturer's instructions, with an added step of a 10-min incubation at 65 °C before the bead-beating step. Libraries were constructed and sequenced as described above, but to an approximate depth of 20 Gbp per total metagenome.

### Soil chemistry and moisture

Soil moisture was defined by calculating the gravimetric water content of the soil. Soil chemistry measurements were performed by Ward Laboratories (Kearney, NE, USA). Briefly, soil pH and soluble salts were measured using a 1:1 soil:water suspension. Soil organic matter was calculated as percent mass loss on ignition. Nitrate was measured using a KCl extraction. Potassium, calcium, magnesium and sodium were measured using an ammonium acetate extraction. Zinc, iron, manganese and copper were measured using a DTPA extraction. Phosphorus was measured using the Olsen method, and sulfate was measured using a Mehlich-3 extraction.

### Virome bioinformatic processing

Reads were trimmed using Trimmomatic v0.39 [50] to remove Illumina adapters and for quality trimming, using paired-end trimming, a sliding window size of 3:40, and a minimum read length of 50 bp. PhiX sequences were removed using BBDuk, from the BBMap v38-72 package [51], using  $k = 31$  and  $hdist = 1$ . De novo assemblies were generated separately for each virome from the quality-trimmed, phiX-free reads, using MEGAHIT v1.0.6 [52], with  $k$ -min of 27, presets meta-large, and a minimum contig length of 1000 bp. It is likely that by using assembly-based approaches for vOTU recovery, heterogeneous viral populations were not sufficiently assembled, and therefore, the viral community diversity may be underestimated [53]. Contigs were renamed, using the rename command from the BBMap package [51], using standard settings, and only contigs ≥ 10 kbp were retained, using reformat from BBMap with the setting `min-length=10000`. Viral contigs were predicted using VIBRANT v1.2.0 [54], in virome mode and retained for downstream analyses if VIBRANT classified the contig as viral. It should be noted that we chose to use only one viral prediction tool, in order to minimize the number of false-positive vOTUs, which means that we likely have missed true-positive viral contigs in our analysis. Viral contigs were dereplicated into vOTUs using dRep v3.2.0 [55] at 95% ANI with a minimum coverage threshold of 85%, using the ANImf algorithm. Reads were mapped to the vOTUs, using Bowtie2 v2.4.2 [56] in sensitive mode (a conservative setting but lacking a specific nucleotide identity cutoff), and the resulting samfiles were converted to bamfiles via SAMtools v1.15.1 [57]. A coverage table was produced using CoverM v0.6.1 [58], using CoverM contig with the mean coverage and a minimum covered fraction (breadth) of 75% (Supplementary Table 4). Reads were

subsequently mapped back to our PIGEONv2.0 database, using CoverM with the same settings.

### Total metagenome bioinformatic processing

Read trimming, PhiX removal, and assembly were done the same way as for the viromes. Contigs were renamed, using the rename command from the BMap package [51], using standard settings, and only contigs  $\geq 2$  kbp were retained, using reformat from BMap with the setting minlength = 2000. CD-HIT v2007-013 [59] was used to deduplicate the contigs at approximately 99% ANI, using the `-c 0.99 -aS 0.99` settings. Bowtie2 v2.4.2 [56] was used to map reads to the contigs, using sensitive mode, and the samfiles were converted to bamfiles using SAMtools v1.15.1 [57]. A depth file for binning was created using MetaBAT2 v2.12.1 [60], using `jgi_summarize_bam_contig_depths`. Bins were then created using MetaBAT2 v2.12.1, using standard settings. dRep v3.2.0 [55] was used to dereplicate the bins, using primary clustering at 90%, secondary clustering at 95%, coverage method larger, a contamination threshold of 5%, and a coverage threshold of 30% [61]. CheckM v1.0.13 [62] was used to estimate completeness and contamination of genome bins, and bins  $\geq 50\%$  complete and  $\leq 10\%$  contaminated were retained [27]. RefineM v0.1.2 [63] was used to refine the recovered bins, using standard settings. Reads were mapped to these bins (metagenome-assembled genomes, MAGs) using Bowtie2 v2.4.2 [56] with default settings, except setting `--min-covered-fraction` to 0.5 [64] (Supplementary Table 5). Phylogenetic trees were constructed using GTDB-Tk v2.1.0 [65], using the `classify-wf` command for phylogenetic inference and for aligning the identified marker genes. After this, GTDB-Tk `infer` was used to create the phylogenetic tree, using standard settings.

### Recovery and analysis of 16S rRNA gene sequences from metagenomes

SortMeRNA v4.2.0 [66] was used against the bacterial and archaeal SILVA databases [67] to recover reads containing 16S rRNA gene sequences from the total soil metagenomes. RDP tools v11 [68] was used to taxonomically classify the sequences, using the RDP database v18 as a reference [69]. A count table of the 16S rRNA gene OTUs was generated using the `hier2phyloseq()` function from the RDPutils package [70].

### PIGEONv2.0

To build upon PIGEON 1.0 [18], we added more viral sequences, mostly from in-house soil data, both published [17, 19, 21, 49] and currently unpublished, and from recent publications of viral ecology in soil [25], lakes [34, 71] and oceans [72, 73]. For each of these vOTUs, the original source environment and original publication is in a table available on Dryad (see Data Availability Statement), but since not all vOTUs had associated metadata and some were detected in multiple samples, researchers are referred to the original publications for additional metadata information. We also mined a total soil (rhizosphere) metagenome dataset for viral sequences [74]. A prefix was added to all sequence headers, in order to quickly identify the dataset from which the original sequence was derived (Supplementary Table 9). All sequences were dereplicated using CD-HIT 2007-0131 [59], because the dataset was too large to use other programs for dereplication. Sequences  $\leq 10$  kbp and  $\geq 500$  kbp were removed. The viromic reads from the current Bodega Bay dataset were also mapped to RefSeq prokaryotic viral genomes ( $n = 2305$ , release 85) [75], according to the read mapping parameters described above, but no RefSeq viral sequences were detected in our dataset. We opted not to add the RefSeq database to PIGEONv2.0, as the RefSeq database is frequently updated, and users may want to use different (newer) versions of RefSeq in combination with PIGEONv2.0.

### Microdiversity profiles

Within-population genetic diversity was calculated using inStrain v1.4.0 [35]. The bam files created by bowtie2 from the viromes were used as input for the inStrain profile option to identify divergent sites for each of the vOTUs. Variants were only called if they had a minimum coverage of 5 reads. MAG population genetic diversity was calculated the same way, using the bam files created by Bowtie2 from the total metagenomes as input for inStrain.

### CRISPR-spacer and iPHoP analyses for virus-host linkages

Crass v1.0.1 [37] was used to assemble spacer and repeat sequences in the total metagenomes, using `-l 4`. All spacer sequences were then compared to the vOTUs, using BLASTn v2.7.1 [76], retaining hits with fewer than two

mismatches, a minimum alignment length of 23 bases, and  $>95\%$  nucleotide identity. All repeat sequences were compared to the MAGs using BLASTn, retaining hits that had no mismatches and 100% nucleotide identity (Supplementary Table 8). Additionally, iPHoP [38] was used to investigate the dataset for additional virus-host linkages, and matches with a confidence score  $\geq 95$  were retained. VIBRANT annotations using the VOG database, based on HMM-based probabilistic searches against the database, were used for the 'predicted viral proteins recovered in CRISPR regions' analysis.

### Data analysis and visualization

All statistical analyses were done using R v 4.1.0 [77]. Analysis for viral community composition were done on the mean coverage vOTU abundance table, unless otherwise noted. Bray-Curtis dissimilarities were calculated on log-transformed relative abundances, using the `vegdist` function from the `vegan` package v2.6-2 [78]. PERMANOVA analyses were done using the `adonis2` function from `vegan`. Principal coordinates analyses were performed with the `pcor` function from `ape` v5.4-2 [79]. The BIO-ENV analysis was done using the `bioenv` function from `vegan`. Co-occurrence analyses for vOTUs, MAGs and 16S rRNA gene OTUs were done using the `coocur` package in R [80], using a presence-absence version of the abundance tables. Only significantly positive co-occurrences ( $p < 0.001$ ) were used for visualization. Co-occurrence networks were visualized using Cytoscape v3.7.1 [81], using the edge-weighted spring embedded model, placing vOTUs that co-occur more frequently in closer proximity to each other in the figure. UpSet plots were created using the UpSetR package v1.4.0 [82], using a presence-absence version of the vOTU abundance table. All maps were created using the R package `ggmaps` [83]. Pie charts and bar charts were created with Python v3.8, using `matplotlib` v3.4.2 [84] and `seaborn` v0.11.2 [85]. The phylogenetic tree was created using the iTOL website [86], and the CRISPR-repeat network linking viruses to hosts was created using Cytoscape. All other plots were created, using the R package `ggplot2` v3.3.5 [87]. Correlation tests between community Jaccard Dissimilarity and spatial or environmental distance were done using the `cor.test()` function, using the Pearson method with the alternative parameter set to two-sided. The linear regression slopes were calculated using the `lm` function, as has been done previously [21]. All scripts are available at <https://github.com/AnneliektH/BodegaBay2021>.

### DATA AVAILABILITY

Raw sequencing reads are available at NCBI under BioProject number PRJNA913601, and sequence processing and statistical analysis code can be found on GitHub (<https://github.com/AnneliektH/BodegaBay2021>). The PIGEONv2.0 database vOTU sequences, the vOTU sequences recovered in this dataset, and MAGs recovered in this dataset are available on Dryad (<https://datadryad.org/>), using the following <https://doi.org/10.25338/B8C934> (datasets with the most recent date stamp are the most current).

### REFERENCES

- Nahlik AM, Fennessy MS. Carbon storage in US wetlands. *Nat Commun.* 2016;7:13835.
- Hopkinson CS, Cai W-J, Hu X. Carbon sequestration in wetland dominated coastal systems—a global sink of rapidly diminishing magnitude. *Curr Opin Environ Sustainability.* 2012;4:186–94.
- Mitsch WJ, Gosselink JG. The value of wetlands: importance of scale and landscape setting. *Ecol Econ.* 2000;35:25–33.
- Mitsch WJ, Bernal B, Hernandez ME. Ecosystem services of wetlands. *Int J Biodivers Sci Eco Services Mgmt.* 2015;11:1–4.
- Yarwood SA. The role of wetland microorganisms in plant-litter decomposition and soil organic matter formation: a critical review. *FEMS Microbiol Ecol.* 2018;94:fyy175.
- Zhou M, Butterbach-Bahl K, Vereecken H, Brüggemann N. A meta-analysis of soil salinization effects on nitrogen pools, cycles and fluxes in coastal ecosystems. *Glob Chang Biol.* 2017;23:1338–52.
- Ardón M, Helton AM, Bernhardt ES. Salinity effects on greenhouse gas emissions from wetland soils are contingent upon hydrologic setting: a microcosm experiment. *Biogeochemistry.* 2018;140:217–32.
- Zhang G, Bai J, Tebbe CC, Zhao Q, Jia J, Wang W, et al. Salinity controls soil microbial community structure and function in coastal estuarine wetlands. *Environ Microbiol.* 2021;23:1020–37.
- Green AJ, Alcorlo P, Peeters ET, Morris EP, Espinar JL, Bravo-Utrera MA, et al. Creating a safe operating space for wetlands in a changing climate. *Front Ecol Environ.* 2017;15:99–107.

10. Dalcin Martins P, Danczak RE, Roux S, Frank J, Borton MA, Wolfe RA, et al. Viral and metabolic controls on high rates of microbial sulfur and carbon cycling in wetland ecosystems. *Microbiome*. 2018;6:138.
11. Emerson JB. Soil viruses: a new hope. *mSystems*. 2019;4:e00120–19.
12. McCalley CK, Woodcroft BJ, Hodgkins SB, Wehr RA, Kim E-H, Mondav R, et al. Methane dynamics regulated by microbial community response to permafrost thaw. *Nature*. 2014;514:478–81.
13. Woodcroft BJ, Singleton CM, Boyd JA, Evans PN, Emerson JB, Zayed AAF, et al. Genome-centric view of carbon processing in thawing permafrost. *Nature*. 2018;560:49–54.
14. Cavicchioli R, Ripple WJ, Timmis KN, Azam F, Bakken LR, Baylis M, et al. Scientists' warning to humanity: microorganisms and climate change. *Nat Rev Microbiol*. 2019;17:569–86.
15. Trubl G, Jang HB, Roux S, Emerson JB, Solonenko N, Vik DR, et al. Soil viruses are underexplored players in ecosystem carbon processing. *mSystems*. 2018;3:e00076–18.
16. Paez-Espino D, Eloe-Fadrosh EA, Pavlopoulos GA, Thomas AD, Huntemann M, Mikhailova N, et al. Uncovering Earth's virome. *Nature*. 2016;536:425–30.
17. Santos-Medellin C, Zinke LA, ter Horst AM, Gelardi DL, Parikh SJ, Emerson JB. Viromes outperform total metagenomes in revealing the spatiotemporal patterns of agricultural soil viral communities. *ISME J*. 2021;15:1956–70.
18. ter Horst AM, Santos-Medellin C, Sorensen JW, Zinke LA, Wilson RM, Johnston ER, et al. Minnesota peat viromes reveal terrestrial and aquatic niche partitioning for local and global viral populations. *Microbiome*. 2021;9:233.
19. Durham DM, Sieradzki ET, ter Horst AM, Santos-Medellin C, Bess CWA, Geonczy SE, et al. Substantial differences in soil viral community composition within and among four Northern California habitats. *ISME Commun*. 2022;2:1–5.
20. Hillary LS, Adriaenssens EM, Jones DL, McDonald JE. RNA-viromics reveals diverse communities of soil RNA viruses with the potential to affect grassland ecosystems across multiple trophic levels. *ISME Commun*. 2022;2:34.
21. Santos-Medellin C, Estera-Molina K, Yuan M, Pett-Ridge J, Firestone MK, Emerson JB. Spatial turnover of soil viral populations and genotypes overlain by cohesive responses to moisture in grasslands. *Proc Natl Acad Sci USA*. 2022;119:e2209132119.
22. Wu R, Davison MR, Nelson WC, Graham EB, Fansler SJ, Farris Y, et al. DNA viral diversity, abundance, and functional potential vary across grassland soils with a range of historical moisture regimes. *mBio*. 2021;12:e0259521.
23. Coclet C, Sorensen PO, Karaoz U, Wang S, Brodie EL, Eloe-Fadrosh EA, et al. Virus diversity and activity is driven by snowmelt and host dynamics in a high-altitude watershed soil ecosystem. *bioRxiv*. 2023. 2023.03.06.531389.
24. Emerson JB, Roux S, Brum JR, Bolduc B, Woodcroft BJ, Jang HB, et al. Host-linked soil viral ecology along a permafrost thaw gradient. *Nat Microbiol*. 2018;3:870–80.
25. Lee S, Sorensen JW, Walker RL, Emerson JB, Nicol GW, Hazard C. Soil pH influences the structure of virus communities at local and global scales. *Soil Biol Biochem*. 2022;166:108569.
26. Roux S, Adriaenssens EM, Dutilh BE, Koonin EV, Kropinski AM, Krupovic M, et al. Minimum Information about an Uncultivated Virus Genome (MIUViG). *Nat Biotechnol*. 2019;37:29–37.
27. Almeida A, Mitchell AL, Boland M, Forster SC, Gloor GB, Tarkowska A, et al. A new genomic blueprint of the human gut microbiota. *Nature*. 2019;568:499–504.
28. Corwin DL, Scudiero E Chapter One - Review of soil salinity assessment for agriculture across multiple scales using proximal and/or remote sensors. In: Sparks DL (ed). *Advances in Agronomy*. 2019. Academic Press, pp 1–130.
29. Bui EN. Causes of soil salinization, sodification, and alkalization. In Oxford Research Encyclopedia of Environmental Science. Oxford University Press: Oxford, UK; 2017. <https://www.oxfordreference.com/display/10.1093/acref/9780190496616.001.0001/acref-9780190496616-e-264>.
30. Shabala S. Learning from halophytes: physiological basis and strategies to improve abiotic stress tolerance in crops. *Ann Bot*. 2013;112:1209–21.
31. Ungar IA. Are biotic factors significant in influencing the distribution of halophytes in saline habitats? *Bot Rev*. 1998;64:176–99.
32. Liang X, Wang Y, Zhang Y, Zhuang J, Radosevich M. Viral abundance, community structure and correlation with bacterial community in soils of different cover plants. *Appl Soil Ecol*. 2021;168:104138.
33. Milanese A, Mende DR, Paoli L, Salazar G, Ruscheweyh H-J, Cuenca M, et al. Microbial abundance, activity and population genomic profiling with mOTUs2. *Nat Commun*. 2019;10:1014.
34. Coutinho FH, Cabello-Yeves PJ, Gonzalez-Serrano R, Rosselli R, López-Pérez M, Zemska TI, et al. New viral biogeochemical roles revealed through metagenomic analysis of Lake Baikal. *Microbiome*. 2020;8:163.
35. Olm MR, Crits-Christoph A, Bouma-Gregson K, Firek BA, Morowitz MJ, Banfield JF. inStrain profiles population microdiversity from metagenomic data and sensitively detects shared microbial strains. *Nat Biotechnol*. 2021;39:727–36.
36. Hanson CA, Fuhrman JA, Horner-Devine MC, Martiny JBH. Beyond biogeographic patterns: processes shaping the microbial landscape. *Nat Rev Microbiol*. 2012;10:497–506.
37. Skennerton CT, Imelfort M, Tyson GW. Crass: identification and reconstruction of CRISPR from unassembled metagenomic data. *Nucleic Acids Res*. 2013;41:e105.
38. Roux S, Camargo AP, Coutinho FH, Dabdoub SM, Dutilh BE, Nayfach S, et al. iPHoP: An integrated machine learning framework to maximize host prediction for metagenome-derived viruses of archaea and bacteria. *PLoS Biol*. 2023;21:e3002083.
39. Meaden S, Biswas A, Arkhipova K, Morales SE, Dutilh BE, Westra ER, et al. High viral abundance and low diversity are associated with increased CRISPR-Cas prevalence across microbial ecosystems. *Curr Biol*. 2022;32:220–7.e5.
40. Hwang Y, Roux S, Coclet C, Krause SJE, Girguis PR. Viruses interact with hosts that span distantly related microbial domains in dense hydrothermal mats. *Nat Microbiol*. 2023;8:946–57.
41. George NA, Hug LA. CRISPR-resolved virus-host interactions in a municipal landfill include non-specific viruses, hyper-targeted viral populations, and interval conflicts. *Sci Rep*. 2023;13:5611.
42. Quinones-Olvera N, Owen SV, McCully LM, Marin MG, Rand EA, Fan AC, et al. Diverse and abundant viruses exploit conjugative plasmids. *bioRxiv*. 2023. <https://doi.org/10.1101/2023.03.19.532758>.
43. Paez-Espino D, Sharon I, Morovic W, Stahl B, Thomas BC, Barrangou R, et al. CRISPR immunity drives rapid phage genome evolution in *Streptococcus thermophilus*. *mBio*. 2015;6:e00262–15.
44. Sun CL, Barrangou R, Thomas BC, Horvath P, Fremaux C, Banfield JF. Phage mutations in response to CRISPR diversification in a bacterial population. *Environ Microbiol*. 2013;15:463–70.
45. Koskella B, Brockhurst MA. Bacteria–phage coevolution as a driver of ecological and evolutionary processes in microbial communities. *FEMS Microbiol Rev*. 2014;38:916–31.
46. Betts A, Gray C, Zelek M, MacLean RC, King KC. High parasite diversity accelerates host adaptation and diversification. *Science*. 2018;360:907–11.
47. Scanlan PD, Hall AR, Lopez-Pascua LDC, Buckling A. Genetic basis of infectivity evolution in a bacteriophage. *Mol Ecol*. 2011;20:981–9.
48. Göller PC, Haro-Moreno JM, Rodriguez-Valera F, Loessner MJ, Gómez-Sanz E. Uncovering a hidden diversity: optimized protocols for the extraction of dsDNA bacteriophages from soil. *Microbiome*. 2020;8:90.
49. Sorensen JW, Zinke LA, ter Horst AM, Santos-Medellin C, Schroeder A, Emerson JB. DNase treatment improves viral enrichment in agricultural soil viromes. *mSystems*. 2021;6:e0061421.
50. Bolger AM, Lohse M, Usadel B. Trimmomatic: a flexible trimmer for Illumina sequence data. *Bioinformatics*. 2014;30:2114–20.
51. Bushnell B BBMap: a fast, accurate, splice-aware aligner. 2014. Lawrence Berkeley National Lab.(LBNL), Berkeley, CA (United States).
52. Li D, Liu C-M, Luo R, Sadakane K, Lam T-W. MEGAHIT: an ultra-fast single-node solution for large and complex metagenomics assembly via succinct de Bruijn graph. *Bioinformatics*. 2015;31:1674–6.
53. Dart E, Fuhrman JA, Ahlgren NA. Diverse marine T4-like cyanophage communities are primarily comprised of low-abundance species including species with distinct seasonal, persistent, occasional, or sporadic dynamics. *Viruses*. 2023;15:581.
54. Kieft K, Zhou Z, Anantharaman K. VIBRANT: automated recovery, annotation and curation of microbial viruses, and evaluation of viral community function from genomic sequences. *Microbiome*. 2020;8:90.
55. Olm MR, Brown CT, Brooks B, Banfield JF. dRep: a tool for fast and accurate genomic comparisons that enables improved genome recovery from metagenomes through de-replication. *ISME J*. 2017;11:2864–8.
56. Longmead B, Salzberg SL. Fast gapped-read alignment with Bowtie2. *Nat Methods*. 2012;9:357–9.
57. Li H, Handsaker B, Wysoker A, Fennell T, Ruan J, Homer N, et al. The Sequence Alignment/Map format and SAMtools. *Bioinformatics*. 2009;25:2078–9.
58. Woodcroft BJ CoverM: Read coverage calculator for metagenomics. Github.
59. Huang Y, Niu B, Gao Y, Fu L, Li W. CD-HIT Suite: a web server for clustering and comparing biological sequences. *Bioinformatics*. 2010;26:680–2.
60. Kang DD, Froula J, Egan R, Wang Z. MetaBAT, an efficient tool for accurately reconstructing single genomes from complex microbial communities. *PeerJ*. 2015;3:e1165.
61. Pasolli E, Asnicar F, Manara S, Zolfo M, Karcher N, Armanini F, et al. Extensive Unexplored Human Microbiome Diversity Revealed by Over 150,000 Genomes from Metagenomes Spanning Age, Geography, and Lifestyle. *Cell*. 2019;176:649–62.e20.
62. Parks DH, Imelfort M, Skennerton CT, Hugenholtz P, Tyson GW. CheckM: assessing the quality of microbial genomes recovered from isolates, single cells, and metagenomes. *Genome Res*. 2015;25:1043–55.

63. Parks DH, Rinke C, Chuvochina M, Chaumeil P-A, Woodcroft BJ, Evans PN, et al. Recovery of nearly 8,000 metagenome-assembled genomes substantially expands the tree of life. *Nat Microbiol.* 2017;2:1533–42.
64. Olm MR, Dahan D, Carter MM, Merrill BD, Yu FB, Jain S, et al. Robust variation in infant gut microbiome assembly across a spectrum of lifestyles. *Science.* 2022;376:1220–3.
65. Chaumeil P-A, Mussig AJ, Hugenholtz P, Parks DH. GTDB-Tk v2: memory friendly classification with the genome taxonomy database. *Bioinformatics.* 2022;38:5315–6.
66. Kopylova E, Noé L, Touzet H. SortMeRNA: fast and accurate filtering of ribosomal RNAs in metatranscriptomic data. *Bioinformatics.* 2012;28:3211–7.
67. Quast C, Pruesse E, Yilmaz P, Gerken J, Schweer T, Yarza P, et al. The SILVA ribosomal RNA gene database project: improved data processing and web-based tools. *Nucleic Acids Res.* 2013;41:D590–6.
68. Wang Q, Garrity GM, Tiedje JM, Cole JR. Naive Bayesian classifier for rapid assignment of rRNA sequences into the new bacterial taxonomy. *Appl Environ Microbiol.* 2007;73:5261–7.
69. Cole JR, Wang Q, Fish JA, Chai B, McGarrell DM, Sun Y, et al. Ribosomal database Project: data and tools for high throughput rRNA analysis. *Nucleic Acids Res.* 2014;42:D633–42.
70. Quensen J RDPutils: R utilities for processing RDPTool output. <https://rdrr.io/github/jfq3/RDPutils/>.
71. Labbé M, Girard C, Vincent WF, Culley AI. Extreme viral partitioning in a marine-derived high arctic Lake. *mSphere.* 2020;5:e00334–20.
72. Vik D, Gazitúa MC, Sun CL, Zayed AA, Aldunate M, Mulholland MR, et al. Genome-resolved viral ecology in a marine oxygen minimum zone. *Environ Microbiol.* 2021;23:2858–74.
73. Li Z, Pan D, Wei G, Pi W, Zhang C, Wang J-H, et al. Deep sea sediments associated with cold seeps are a subsurface reservoir of viral diversity. *ISME J.* 2021;15:2366–78.
74. Xu J, Zhang Y, Zhang P, Trivedi P, Riera N, Wang Y, et al. The structure and function of the global citrus rhizosphere microbiome. *Nat Commun.* 2018;9:4894.
75. Pruitt KD, Tatusova T, Maglott DR. NCBI reference sequences (RefSeq): a curated non-redundant sequence database of genomes, transcripts and proteins. *Nucleic Acids Res.* 2007;35:D61–5.
76. Altschul SF, Gish W, Miller W, Myers EW, Lipman DJ. Basic local alignment search tool. *J Mol Biol.* 1990;215:403–10.
77. RCore T. R: A language and environment for statistical computing. R Foundation for Statistical Computing, Vienna, Austria. 2016.
78. Oksanen J, Blanchet FG, Friendly M, Kindt R, Legendre P, McGlenn D, et al. *vegan: Community Ecology Package.* R package version 2.5-2. 2018. 2018. Vienna: R Core Team.
79. Paradis E, Schliep K. *ape 5.0: an environment for modern phylogenetics and evolutionary analyses in R.* *Bioinformatics.* 2019;35:526–8.
80. Griffith DM, Veech JA, Marsh CJ. *cooccur: probabilistic species co-occurrence analysis in R.* *J Stat Softw.* 2016;69:1–17.
81. Shannon P, Markiel A, Ozier O, Baliga NS, Wang JT, Ramage D, et al. Cytoscape: a software environment for integrated models of biomolecular interaction networks. *Genome Res.* 2003;13:2498–504.
82. Conway JR, Lex A, Gehlenborg N. *UpSetR: an R package for the visualization of intersecting sets and their properties.* *Bioinformatics.* 2017;33:2938–40.
83. Kahle D, Wickham H *ggmap: Spatial visualization with ggplot2.* *The R J.* 5, 144–61. <https://www.journalr-project.org/archive/2013-1/kahle>.
84. Hunter. *Matplotlib. A 2D Graphics Environment.* 2007;9:90–5.
85. *seaborn: statistical data visualization — seaborn 0.11.2 documentation.* <https://seaborn.pydata.org/>.
86. Letunic I, Bork P. Interactive tree of life (iTOL) v5: an online tool for phylogenetic tree display and annotation. *Nucleic Acids Res.* 2021;49:W293–96.
87. Wickham H *ggplot2: elegant graphics for data analysis.* *data.* 2016.

## ACKNOWLEDGEMENTS

We thank Sara Geonczy and Devyn Durham for their help with sampling, Christian Santos-Medellin for helpful discussions, and the University of California, Davis Natural Reserves site directors and staff, particularly Suzanne Olyarnik at the Bodega Marine Reserve, for facilitating site access and providing logistical support. Funding for this work was provided by the U.S. Department of Energy (DOE), Office of Science, Office of Biological and Environmental Research (BER), Genomic Science Program, award number DE-SC0021198 (grant to JBE).

## AUTHOR CONTRIBUTIONS

JE and AH designed the experiments. JF, JS and AH collected samples for this study, with JS providing information about the plant community at field sites. AH performed laboratory work and analyzed the data. JE and AH wrote the manuscript.

## COMPETING INTERESTS

The authors declare no competing interests.

## ADDITIONAL INFORMATION

**Supplementary information** The online version contains supplementary material available at <https://doi.org/10.1038/s41396-023-01516-8>.

**Correspondence** and requests for materials should be addressed to Joanne B. Emerson.

**Reprints and permission information** is available at <http://www.nature.com/reprints>

**Publisher's note** Springer Nature remains neutral with regard to jurisdictional claims in published maps and institutional affiliations.

Springer Nature or its licensor (e.g. a society or other partner) holds exclusive rights to this article under a publishing agreement with the author(s) or other rightsholder(s); author self-archiving of the accepted manuscript version of this article is solely governed by the terms of such publishing agreement and applicable law.